Eur. Phys. J. B (2017) 90: 92
DOI: 10.1140/epjb/e2017-80038-3

THE EUROPEAN PHYSICAL JOURNAL B

Regular Article

Strain engineering of graphene nanoribbons: pseudomagnetic versus external magnetic fields

Sanjay Prabhakar[1,a], Roderick Melnik[1,2], and Luis Bonilla[3]

[1] The MS2Discovery Interdisciplinary Research Institute, M2NeT Laboratory, Wilfrid Laurier University, Waterloo, ON, N2L 3C5, Canada
[2] BCAM-Basque Center for Applied Mathematics, 48009 Bilbao, Spain
[3] Gregorio Millan Institute, Fluid Dynamics, Nanoscience and Industrial Mathematics, Universidad Carlos III de Madrid, 28911 Leganes, Spain

Received 15 January 2017 / Received in final form 27 March 2017
Published online 17 May 2017 –

Abstract. Bandgap opening due to strain engineering is a key architect for making graphene's optoelectronic, straintronic, and spintronic devices. We study the bandgap opening due to strain induced ripple waves and investigate the interplay between pseudomagnetic fields and externally applied magnetic fields on the band structures and spin relaxation in graphene nanoribbons (GNRs). We show that electron-hole bands of GNRs are highly influenced (i.e. level crossing of the bands are possible) by coupling two combined effects: pseudomagnetic fields (PMF) originating from strain tensor and external magnetic fields. In particular, we show that the tuning of the spin-splitting band extends to large externally applied magnetic fields with increasing values of pseudomagnetic fields. Level crossings of the bands in strained GNRs can also be observed due to the interplay between pseudomagnetic fields and externally applied magnetic fields. We also investigate the influence of this interplay on the electromagnetic field mediated spin relaxation mechanism in GNRs. In particular, we show that the spin hot spot can be observed at approximately $B = 65$ T (the externally applied magnetic field) and $B_0 = 53$ T (the magnitude of induced pseudomagnetic field due to ripple waves) which may not be considered as an ideal location for the design of straintronic devices. Our analysis might be used for tuning the bandgaps in strained GNRs and utilized to design the optoelectronic devices for straintronic applications.

1 Introduction

Graphene has attracted increasing interest for the design of optoelectronic devices because it possesses unique electronic properties due to the presence of Dirac-like energy spectrum of the charge carriers [1–4]. Several observed quantum phenomena such as the half integer quantum Hall effect, non-zero Berry phase, as well as the measurement of conductivity of electrons in the electronic devices lead to novel applications in carbon based nanoelectronic devices [1–3,5–7]. The experimental data observed by the quantum Hall effect measurement technique suggest that a one atom thick graphene sheet has the same properties as a two dimensional system that does not contain any bandgap at two Dirac points [3]. In addition, the researchers around the globe desire to build next generation semiconductor devices from graphene because the experimental data show that the electronic mobility of this material is very high. In such devices, one finds an opportunity to control electronic properties of graphene-based structures using several different techniques such as gate controlled electric fields and magnetic fields. Further, one can engineer the straintronic devices by controlling the electromechanical properties via the pseudomorphic gauge fields [8–12].

Two dimensional images of a graphene sheet taken from high resolution transmission electron microscope or scanning tunneling microscope show that its surface normal varies by several degrees and the out-of-plane deformations reach to the nanometer scale that is considered to be due to the presence of ripple waves in graphene sheets [13–15]. Ripples in graphene are induced by several different mechanisms that have been widely investigated [8,11,14,16–22]. Such ripples are part of the intrinsic properties of graphene that are expected to strongly affect the band structures due to their coupling through pseudomorphic vector potential [10,12,23]. Monte-Carlo simulation results show that the ripples spontaneously appear owing to thermal fluctuations with a size distribution due to the multiplicity of chemical bonding in carbon [24]. Recent experimental studies on graphene at several different annealed temperatures confirmed that the amplitude of the ripple waves is enhanced with increasing temperature [12]. In experiments on graphene suspended on

[a] e-mail: sprabhakar@wlu.ca

substrate trenches, there appear much longer and taller waves (close to a micron scale) directed parallel to the applied stress. These long wrinkles can also be induced thermally [12]. Recent experimental and theoretical findings utilize small spin-orbit coupling to estimate decoherence time for the prospect of transporting spin information over long distances in graphene for spintronics applications [25–27]. In this paper we present a model that couples the Navier equations, accounting for electromechanical effects, to the electronic properties of armchair and zigzag graphene nanoribbons. We show that the ripple waves, originating from the electromechanical effects, strongly influence the band structures of GNRs. This response mechanism might be used for tuning the bandgaps at the Dirac point in strained GNRs and the numerical estimate of electromagnetic field mediated spin transition rate in such strained GNRs can be utilized to design the optoelectronic devices for the application in straintronics.

The paper is organized as follows: in Section 2, we provide a theoretical description of coupling between the electromechanical effects and the band structures of armchair and zigzag GNRs. Here we show that the energy spectrum of GNRs is highly sensitive to the ripples waves. Numerical schemes for evaluating the influence of electromechanical effects on the band structures calculation of GNRs via exact diagonalization technique is discussed in Section 3. In this section, we also discuss the results on the electromechanical effects and band structures of strained GNRs and estimate the spin relaxation times mediated by electromagnetic field. Finally, we summarize our results in Section 4.

2 Theoretical model

The total elastic energy density associated with the strain for the two dimensional graphene sheet can be written as [18,19,28] $2U_s = C_{iklm}\varepsilon_{ik}\varepsilon_{lm}$. Here C_{iklm} is a tensor of rank four (the elastic modulus tensor) and ε_{ik} (or ε_{lm}) is the strain tensor. In the above, the strain tensor components can be written as

$$\varepsilon_{ik} = \frac{1}{2}\left(\partial_{x_k}u_i + \partial_{x_i}u_k + \partial_{x_k}h\partial_{x_i}h\right), \tag{1}$$

where u_i and h are in-plane and out-of-plane displacements, respectively [8,12,18,23,29]. Hence, the strain tensor components for graphene in the 2D displacement vector $\mathbf{u}(x,y) = (u_x, u_y)$ can be written as

$$\varepsilon_{xx} = \partial_x u_x + \frac{1}{2}\left(\partial_x h\right)^2, \tag{2}$$

$$\varepsilon_{yy} = \partial_y u_y + \frac{1}{2}\left(\partial_y h\right)^2, \tag{3}$$

$$\varepsilon_{xy} = \frac{1}{2}\left(\partial_y u_x + \partial_x u_y\right) + \frac{1}{2}\left(\partial_x h\right)\left(\partial_y h\right). \tag{4}$$

The stress tensor components $\sigma_{ik} = \partial U_s/\partial\varepsilon_{ik}$ for graphene can be written as

$$\sigma_{xx} = C_{11}\varepsilon_{xx} + C_{12}\varepsilon_{yy}, \tag{5}$$

$$\sigma_{yy} = C_{12}\varepsilon_{xx} + C_{22}\varepsilon_{yy}, \tag{6}$$

$$\sigma_{xy} = 2C_{66}\varepsilon_{xy}. \tag{7}$$

In the continuum limit, elastic deformations of graphene sheets under applied tensions are described by the Navier equations $\partial_j\sigma_{ik} + F_i/t = 0$, where F_i are applied tensions. Hence, the coupled Navier equations of electroelasticity can be written as [28]:

$$\begin{aligned}\left(C_{11}\partial_x^2 + C_{66}\partial_y^2\right)u_x + \left(C_{12}+C_{66}\right)\partial_x\partial_y u_y \\ + \frac{1}{2}\partial_x\left[C_{11}\left(\partial_x h\right)^2 + C_{12}\left(\partial_y h\right)^2\right] \\ + C_{66}\partial_y\left(\partial_x h\right)\left(\partial_y h\right) + \frac{F_x}{t} = 0,\end{aligned} \tag{8}$$

$$\begin{aligned}\left(C_{66}\partial_x^2 + C_{11}\partial_y^2\right)u_y + \left(C_{12}+C_{66}\right)\partial_x\partial_y u_x \\ + \frac{1}{2}\partial_y\left[C_{12}\left(\partial_x h\right)^2 + C_{22}\left(\partial_y h\right)^2\right] \\ + C_{66}\partial_x\left(\partial_x h\right)\left(\partial_y h\right) + \frac{F_y}{t} = 0,\end{aligned} \tag{9}$$

where t is the thickness of the single layer graphene, $F_x = \tau_e q\sin(qx)$ and $F_y = \tau_e q\sin(qy)$. Here $q = 2\pi/\iota$ with ι being the period length of the in-plane ripple waves and τ_e is the externally applied tensile edge stress. We assume symmetric out-of-plane ripple waves ($\partial_x h = kh_0\cos kx, \partial_y h = kh_0\cos ky$, where $k = 2\pi/\ell$, ℓ is the period and h_0 is the height of out-of-plane ripple waves) travel along x and y direction in the plane of two dimensional graphene sheet [12,30,31]. Thus, we write equations (8) and (9) as:

$$\begin{aligned}&\left(C_{11}\partial_x^2 + C_{66}\partial_y^2\right)u_x + \left(C_{12}+C_{66}\right)\partial_x\partial_y u_y \\ &= \frac{1}{2}C_{11}k^3h_0^2\sin(2kx) \\ &\quad + C_{66}k^3h_0^2\cos(kx)\sin(ky) - \frac{\tau_e q}{t}\sin(qx),\end{aligned} \tag{10}$$

$$\begin{aligned}&\left(C_{66}\partial_x^2 + C_{11}\partial_y^2\right)u_y + \left(C_{12}+C_{66}\right)\partial_x\partial_y u_x \\ &= \frac{1}{2}C_{22}k^3h_0^2\sin(2ky) \\ &\quad + C_{66}k^3h_0^2\sin(kx)\cos(ky) - \frac{\tau_e q}{t}\sin(qy).\end{aligned} \tag{11}$$

In this paper, we are interested to investigate the influence of ripple waves traveling along y-direction on the band structures of elongated graphene nanoribbons in x-direction. Thus in this case, we assume zigzag GNRs elongated along x-direction with applied tensile edge stress along y-direction that induce ε_{yy} is a non-vanishing strain tensor component. Thus, we write equation (9) as [30]:

$$\varepsilon_{yy} = \varepsilon_s\left(1 + \varepsilon_s'\cos(qy)\right), \tag{12}$$

where $\varepsilon_s' = \tau_e/c_{22}t\varepsilon_s$ and

$$\varepsilon_s = \frac{1}{4}k^2h_0^2 + \frac{kh_0^2}{4L}\sin(kL) - \frac{2\tau_e}{qc_{22}tL}\sin\left(\frac{qL}{2}\right). \tag{13}$$

Now we turn to the influence of strain tensor on the electronic properties of graphene nanoribbons.

In the continuum limit, by expanding the momentum close to the K point in the Brillouin zone, the Hamiltonian for π electrons at the K point reads as [2,32,33]:

$$H = v_F \left(\tau_x P_x + \tau_y P_y\right). \tag{14}$$

In equation (14), $P = p - \hbar A_s - eA$ with $p = -i\hbar\partial_x$ being the canonical momentum operator, $\mathbf{A_s} = (-\varepsilon_{yy}, 0)\,\beta/a$ is the vector potential induced by pseudomorphic strain tensor [34], $\mathbf{A} = B(-y, 0)$ is the vector potential due to applied magnetic field, B, along z-direction and Pauli matrices τ_x and τ_y acting on sublattice or corresponds to pseudospin degree of freedom [17,29,31,35]. We consider that applied magnetic field does not break the time reversal symmetry and thus Zeeman spin energy has been neglected. In (14), we do not consider the valley degree of freedom due to the fact that the strained zigzag graphene nanoribbon does not see the admixture of wavefunctions from different valleys [2,36]. For the armchair graphene nanoribbon, valley degree of freedom can not be ignored [2,37]. We may also apply tensile edge stress along the x-direction and consider ε_{xx} as a non-vanishing strain tensor component. However, for this specific case, we find $[\mathrm{H},\varepsilon_{xx}] = 0$. Thus, the x-component of the strain tensor does not induce any quantum confinement effects and may not present much interest for the band engineering applications.

For strained graphene nanoribbons with zigzag edge, we solve $H\psi = \varepsilon\psi$, where

$$\psi(r) = \exp(ik_x x)\left(\phi_A(y)\ \ \phi_B(y)\right)^T \ [38].$$

Thus, the two coupled equations can be written as

$$\left(k_x - \partial_y + \frac{\beta}{a}\varepsilon_{yy} + \frac{eB}{\hbar}y\right)\phi_B = \left(\frac{\varepsilon}{\hbar v_F}\right)\phi_A, \tag{15}$$

$$\left(k_x + \partial_y + \frac{\beta}{a}\varepsilon_{yy} + \frac{eB}{\hbar}y\right)\phi_A = \left(\frac{\varepsilon}{\hbar v_F}\right)\phi_B. \tag{16}$$

Now, we can apply the operator $(k_x + \partial_y + \frac{\beta}{a}\varepsilon_{yy} + \frac{eB}{\hbar}y)$ from left on (15) and the operator $(k_x - \partial_y + \frac{\beta}{a}\varepsilon_{yy} + \frac{eB}{\hbar}y)$ from left on (16) and cast these two coupled equations (15) and (16) in two decoupled equations for sublattices A and B as:

$$\begin{aligned}(\hbar v_F)^2\Big[-\partial_y^2 + \left(\frac{\beta}{a}\right)^2\varepsilon_{yy}^2 + \left(\frac{eB}{\hbar}\right)^2 y^2 \\ \mp \frac{\beta\tau_e q}{aC_{22}t}\sin(qy) \pm \frac{eB}{\hbar} + k_x^2 + 2\frac{\beta}{a}\varepsilon_{yy}k_x + 2\frac{eB}{\hbar}k_x y \\ + 2\frac{\beta}{a}\frac{eB}{\hbar}\varepsilon_{yy}y\Big]\phi_{B,A} = \varepsilon^2\phi_{B,A}.\end{aligned} \tag{17}$$

In equation (17), we have used the identity: $[\partial_y\varepsilon_{yy} - \varepsilon_{yy}\partial_y] = -\tau_e q\sin(qy)/C_{22}t$ and, $[\partial_y, y] = 1$. In the model equation (17) for strained GNRs in presence of external magnetic field, it is clear that the interplay between pseudo-spin due to applied tensile edge stress, τ_e, and external magnetic field, B, can influence the band diagram of GNRs. Now, we analyze these coupled effects (pseudo-fields and magnetic fields) on the band structures of GNRs with several control parameters: τ_e (applied stress), h_0 (amplitude of out-of-plane ripple waves), L (GNRs width) and B (external magnetic field).

3 Results and discussions

We assume that strain tensor induces a parabolic confinement potential in (17) and thus we apply the vanishing boundary conditions for the wavefunctions ϕ_A and ϕ_B at the two boundaries. Whether the vanishing boundary conditions are appropriate for GNRs of widths $L = 3\sqrt{3}aN$ with $N = 60$ or not, we assume $\cos(qy) \approx 1 - q^2y^2/2$ and expand

$$\varepsilon_{yy}^2 = \varepsilon_0\left(1 - \varepsilon_0' q^2 y^2\right), \tag{18}$$

where $\varepsilon_0 = \varepsilon_s^2(1+\varepsilon_s')^2$ and $\varepsilon_0' = \varepsilon_s'/(1+\varepsilon_s')$. Now we estimate $(\beta/a)^2\varepsilon_0\varepsilon_0' q^2y^2 \approx 31 \gg 0$ (0 is a case for unstrained graphene) for $L = 3\sqrt{3}aN$ with $N = 50$ at $x = \pm L/2$. Such a large confinement potential due to strain effect provides a reseasonable assumption for vanishing boundary conditions of the wavefunctions associated with (17). We diagonalize the Dirac Hamiltonian by utilizing the finite element method[1]. For GNRs considered here, typical numbers of elements depend on grid refinements and exceed 6500. We solve the multiphysics problem i.e., coupling electroelasticity theory in the band diagram of graphene, ensuring the convergence of the results. In Figure 1, we have plotted the band diagram of strained graphene nanoribbons for electron-hole states at $\tau_e = 100$ eV/nm, $h_0 = 1$ nm and $B = 65$ T and $L = 44.27$ nm. The influence of strain and external magnetic fields can be seen clearly at the zero energy band near the Dirac points as well as at higher energies near the band center [36,39]. Here we see that the bands are splitted due to externally applied magnetic fields. The interplay between pseudomagnetic fields due to non-vanishing strain tensor and external magnetic fields provides two fold degenerate bands at $k_x = 0$ that is lifted for $k_x \neq 0$.

In Figure 2, we have plotted the band structures of strained graphene nanoribbons of electron-hole states vs. magnetic fields at Dirac point ($k_x = 0$). Here we find that the band splitting of GNRs can be observed at $B \approx 40$ T and the level crossing of the band can be seen at $B \approx 80$ T due to the interplay between pseudo-fields originating from strain tensor and external magnetic fields. To understand the mechanism of level crossing of the bands, it is important to find an analytical expression for the energy eigenvalues of sublattices A and B from equation (17).

[1] Comsol Multiphysics (www.comsol.com).

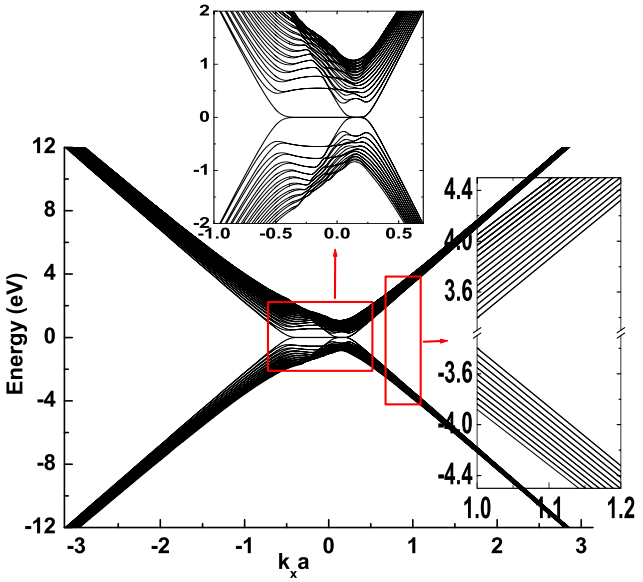

Fig. 1. Band structures of strained graphene nanoribbons of electron-hole states for $L = 3\sqrt{3}aN$ with $N = 60$. The parameters are chosen as: $\tau_e = -100$ eV/nm, $h_0 = 1$ nm, $L = 3\sqrt{3}aN$ with $N = 60$, $a = 0.142$ nm, $B = 65$ T, $\ell = 3.5L$ and $\iota = L$. The interplay between pseudo-spin (due to strain tensor) and external magnetic fields comes into effect largely at $k_x \neq 0$.

Thus we express (17) as:

$$\left[\frac{p_y^2}{2m_0} + \frac{1}{2}m_0\omega_0^2 y^2 + \delta_{\mp} y\right]\phi_{B,A} = \frac{1}{2m_0 v_F^2}[\varepsilon^2 \mp eB\hbar v_F^2 - \frac{1}{4}(g_0\mu_B B)^2 - \left(\frac{\beta}{a}\right)^2 \varepsilon_s^2 (1+\varepsilon_s')^2 (\hbar v_F)^2]\phi_{B,A}, \tag{19}$$

where,

$$\omega_0 = \frac{\hbar}{m_0}\left[\left(\frac{eB}{\hbar}\right)^2 - \left(\frac{\beta}{a}\right)^2 \varepsilon_s^2 (1+\varepsilon_s')\varepsilon_s' q^2\right]^{1/2}. \tag{20}$$

$$\delta_{\mp} = \frac{\hbar^2}{2m_0}\left[\frac{2\beta eB}{a\hbar}(\varepsilon_s + \varepsilon_s\varepsilon_s') \mp \frac{\beta\tau_e q^2}{ac_{22}t}\right]. \tag{21}$$

Energy spectrum of (19) can be written as:

$$\varepsilon_n^2 = 2m_0 v_F^2\left[\left(n+\frac{1}{2}\right)\hbar\omega_0 + \varepsilon_n^{(2)}\right] \pm \frac{eB}{\hbar}(\hbar v_F)^2 + \frac{1}{4}(g_0\mu_B B)^2 + \left(\frac{\beta}{a}\right)^2 \varepsilon_s^2 (1+\varepsilon_s')^2 (\hbar v_F)^2, \tag{22}$$

where $\varepsilon_n^{(2)}$ is the second order energy correction due to $\delta_{\mp} y$ in (19). For example, first order energy correction term of ground state energy eigenvalues of sublattices B and A can be written as:

$$\varepsilon_0^{(2)} = -\frac{|\delta_{\mp}|^2}{2m_0\omega_0^2}, \tag{23}$$

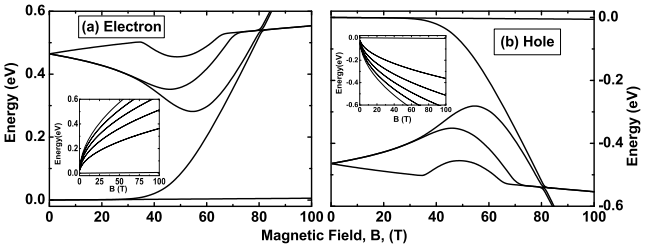

Fig. 2. Band structures of strained graphene nanoribbons of electron-hole states vs. magnetic fields at Dirac point ($k_x = 0$). The band splitting can be seen at $B \approx 40$ T and the band crossing can be seen at $B \approx 80$ T. The parameters are chosen to be the same as Figure 1.

where $\pm$ sign corresponds to the energy eigenvalues associated to the wavefunctions, ϕ_B and ϕ_A. This confirms that the difference in energy eigenvalues between sublattices B and A is enhanced by considering the combined effect of strain and applied magnetic field that gives an indication of electron and hole bands splitting. From equation (22), it is also clear that ground state energy eigenvalues of sublattice B are increased with magnetic field while first excited state energy eigenvalues of sublattice A are decreased with magnetic field. Thus, a level crossing point is expected at appropriate values of applied magnetic field in strained GNRs which is reflected in the numerical simulation results in Figure 2. Such band splitting of sublattices A and B of GNRs can be recognized as pseudo-Landau levels. Indeed, if the applied strain is weak or if we are considering unstrained graphene nanoribbons then one can not observe such conduction and valence band splitting which is clearly seen in the inset plot of Figure 2. The localized states of the pseudo-Landau levels are terminated to the edge of the zigzag GNRs due to the fact that the strain tensor acts like a displaced parabolic potential that transports the localized states to the edge and can be understood in terms of pseudo-Landau edge states [40,41]. In other words, distribution and polarity of pseudomagnetic field throughout the graphene nanoribbon can be found as: $\mathbf{B_s} = \nabla \times \mathbf{A_s} = B_0 \cos(qy)$, where $B_0 = -2\pi\hbar\beta\tau_e q/ec_{22}ta$ is the strength of the PMF due to ripple waves. By choosing the parameters listed in Figure 2, we estimate $B_0 \approx 2600$ T (twice as large as in reference [42] but resembles to the value obtained in reference [43]) as the strength of PMF. Such large PMF value is experimentally feasible in graphene and widely investigated [30,34,43]. Hence such a large PMF originating from ripple waves induces a persistent current that is transported from the center to the edge of the graphene nanoribbon. As a result, the electron-hole states wavefunction drifts towards and over the edge of graphene sheet and provides edge states pseudomagnetic Landau levels [40,41]. To analyze how much external magnetic field alone has contributed on the bands of GNRs at Dirac K point, we consider $\varepsilon_{yy} = 0$ and write (22) as:

$$\varepsilon_n^2 = 2m_0 v_F^2\left(n+\frac{1}{2}\right)\hbar\omega_0 \pm m_0\hbar\omega_0 v_F^2 + \frac{1}{4}(g_0\mu_B B)^2, \tag{24}$$

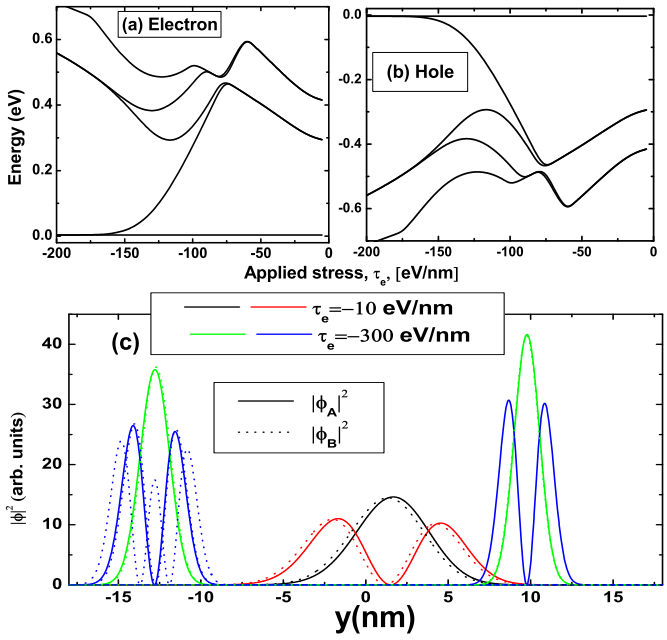

Fig. 3. Band structures of strained graphene nanoribbons of electron-hole states vs. externally applied tensile edge stress at Dirac point ($k_x = 0$). The band splitting can be seen between $\tau_e \approx -55$ eV/nm and –150 eV/nm. For $\tau_e < -55$ eV/nm, we do not find any band splitting. For $\tau_e > -150$ eV/nm, we find all bands located at the zigzag edge. The parameters are chosen to be the same as Figure 1.

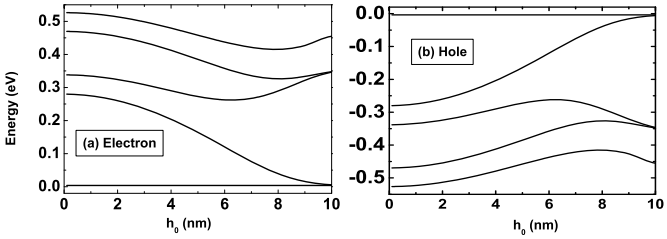

Fig. 4. Band structures of strained graphene nanoribbons of electron-hole states vs. amplitude of out-of-plane displacement vector at Dirac point ($k_x = 0$). The spin splitted bands collapse to a single band at $h_0 = 10$ nm. The parameters are chosen to be the same as Figure 1.

where $\omega_0 = eB/m_0$. We have plotted several energy bands vs. magnetic fields in inset plot of Figure 2 for unstrained GNRs. It can be seen that the parabolic confinement potential induced by external applied magnetic fields induce zero modes that provide us the flat band in the bandstructure of GNRs. From this inset plot, it is clear that band crossing with magnetic field alone in unstrained GNRs is not possible. This motivates us to manipulate graphene spins in Figure 2 with magnetic fields in presence of in-plane and out-of-plane ripple waves for straintronic and spintronic applications.

In Figure 3, we have plotted the energy bands vs. applied tensile edge stress in presence of externally applied magnetic field at $B = 65$ T. For $\tau_e < -75$ eV/nm, the energy bands induced by the external magnetic field is much stronger than the pseudomagnetic field and thus one can not find the splitting of the bands. The strength of the pseudomagnetic field is characterized by $B_s = \nabla \times A_s = B_0 \sin(qy)$, where $B_0 = 2\pi\hbar\beta\tau_e q/aC_{22}t$ and the pseudo-vector potential $A_s = -\beta(\varepsilon_{yy}, 0)/a$. For $\tau_e > -75$ eV/nm, the interplay between pseudomagnetic fields and external magnetic fields comes into effect and thus, combining these two fields in the graphene's Hamiltonian, induces splitting of GNRs bands. At large externally applied tensile edge stress, $\tau_e > -150$ eV/nm, pseudomagnetic potential acts like a displaced double parabolic potential that induces confined localized edge states which exist near the edge of zigzag GNRs (see Fig. 3c). The dotted lines in Figure 3c shows the probability distribution of electron wavefunctions of the sublattice B. Similar prediction of the localization of electron-hole wavefunctions near the zigzag edge was shown in Figure 2d of reference [38] by utilizing tight binding approximation. The interplay between the states formed at the center of the ribbon due to magnetic confinement potential and the edge states due to strain tensor induces the level crossing of the graphene bands at $\tau_e > -150$ eV/nm. In Figure 4, we have plotted the energy bands vs. amplitude of the out-of-plane ripple waves at $\tau_e = -100$ eV/nm and $B = 65$ T. Here we again see that the interplay between pseudo-potential due to out-of-plane ripple waves and magnetic field induces level crossing of the bands at $h = 10$ nm.

In Figure 5, we have plotted spin-splitting energy difference vs. magnetic fields by varying externally applied tensile edge stress at $h_0 = 1$nm. In Figure 5a, we see that the level crossing point due to the interplay between pseudomagnetic fields originating from electromechanical effects and externally applied magnetic fields along z-direction can be observed at $B = 37$ T for $\tau_e = -30$ eV/nm. In Figures 5a and 5b, we also find that the tuning of level crossing point extends to larger magnetic fields with increasing values of applied tensile edge stress. From Figures 5a and 5b, it is clear that the level crossing point with magnetic field is inversely proportional to the graphene nanoribbon widths. For $\tau_e = -30$ eV/nm, we find the level crossing point at $B = -37$ T in Figure 5a for GNRs width, $L = 3\sqrt{3}aN$ with $N = 50$ and $B = 25$ T in Figure 5b for GNRs width, $L = 3\sqrt{3}aN$ with $N = 70$. Thus, we can conclude that the tuning of the level crossing point extends to larger magnetic fields with decreasing graphene nanoribbon widths which is reflected in Figures 5a and 5b.

We now turn to the calculations of the transition rate between the two energy levels due to spontaneous emission of photons. In presence of electromagnetic field radiation, we replace momentum operator P by $P = p - \hbar A_s - eA - eA_{em}(r,t)$, where $A_{em}(r,t)$ is the additional vector potential induced by electromagnetic field radiation and write the total Hamiltonian of graphene as $\tilde{H} = H + H_A$, where H_A is the additional contribution in the Hamiltonian of graphene due to the electromagnetic field radiation of photons that can be written as

$$H_A = -ev_F\left(A_-\tau_+ + A_+\tau_-\right), \qquad (25)$$

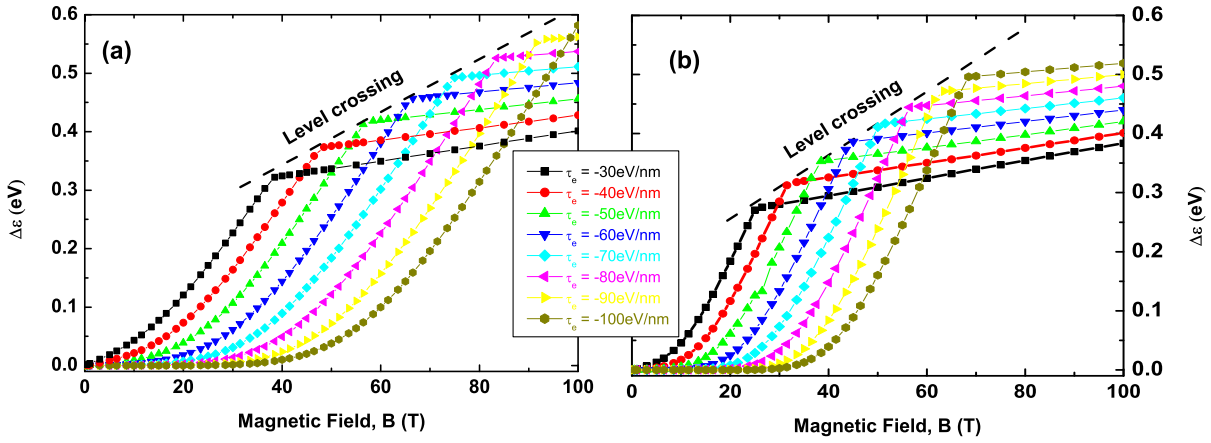

Fig. 5. Spin splitting energy difference ((left) $L = 3\sqrt{3}aN$ with $N = 50$ and (right) $L = 3\sqrt{3}aN$ with $N = 70$) vs. magnetic field at Dirac point ($k_x = 0$). Level crossing is clearly seen due to interplay between pseudomagnetic fields characterized by τ_e and magnetic field, B. The parameters are chosen to be the same as Figure 1.

where $\tau_\pm = (\tau_x \pm i\tau_y)/2$ and $A_\pm = A_x \pm iA_y$. Here A_x and A_y are the components of the vector potential $\mathbf{A_{em}}(\mathbf{r}, t)$ of the electromagnetic field radiation of photons that can be written as

$$\mathbf{A_{em}}(\mathbf{r}, t) = \sum_{q,\lambda} \sqrt{\frac{\hbar}{2\epsilon_r \omega_\mathbf{q} V}} \hat{e}_{q\lambda} b_{q,\lambda} e^{i(\mathbf{q}\cdot\mathbf{r} - \omega_q t)} + H.c., \quad (26)$$

where $\omega_q = c|\mathbf{q}|$, $b_{q,\lambda}$ annihilate photons with wave vector $\mathbf{q}$, c is the velocity of light, V is the volume and ϵ_r is the dielectric constant of the graphene nanoribbon. The polarization directions $\hat{e}_{\mathbf{q}\lambda}$ with $\lambda = 1, 2$ are chosen as two perpendicular induced photon modes in the graphene nanoribbon. The polarization directions of the induced photons are $\hat{e}_{q1} = (\sin\phi, -\cos\phi, 0)$ and $\hat{e}_{q2} = (\cos\theta\cos\phi, \cos\theta\sin\phi, -\sin\theta)$ because we express $\mathbf{q} = q(\sin\theta\cos\phi, \sin\theta\sin\phi, \cos\theta)$. The above polarization vectors satisfy the relations $\hat{e}_{q1} = \hat{e}_{q2} \times \hat{\mathbf{q}}$, $\hat{e}_{q2} = \hat{\mathbf{q}} \times \hat{e}_{q1}$ and $\hat{\mathbf{q}} = \hat{\mathbf{e}}_{\mathbf{q1}} \times \hat{\mathbf{e}}_{\mathbf{q2}}$. Based on the Fermi Golden Rule, the electromagnetic field mediated transition rate (i.e., the transition probability per unit time) in the graphene nanoribbon is given by [44]

$$\frac{1}{T_1} = \frac{V}{(2\pi)^2 \hbar} \int d^3\mathbf{q} \sum_{\lambda=1,2} |M_{q,\lambda}|^2 \delta(\hbar\omega_\mathbf{q} - \varepsilon_f + \varepsilon_i), \quad (27)$$

where $M_{q,\lambda} = \langle\psi_i|H_A|\psi_f\rangle$. Here $|\psi_i\rangle$ and $|\psi_f\rangle$ are the initial and final states wavefunctions. By adopting the dipole approximation, i.e. the transition is caused only by leading terms from $A(\mathbf{r}, t)$, we investigate the influence of interplay between externally applied magnetic field and pseudomagnetic field due to ripples waves on the electromagnetic field mediated spin relaxation mechanism of graphene nanoribbons in Figure 6. In Figure 6a, we have plotted the transition rate between several energy eigenvalues (see the schematic diagram in the inset plot and the real band diagram in Fig. 2) vs. externally applied magnetic field. Here we find that at large magnetic field, $B \approx 65$ T, the level crossing due to admixture of spin and orbital states greatly enhances the spin-relaxation rate. Hence, the relaxation rate can approach to the orbital relaxation rate due to the level crossing of orbital and spin states. One may estimate the decoherence time $T_2 \approx 2T_1$ and can predict that the decoherence time is much smaller due to admixture of spin and orbital states at the level crossing point that can be considered as a spin hot spot.

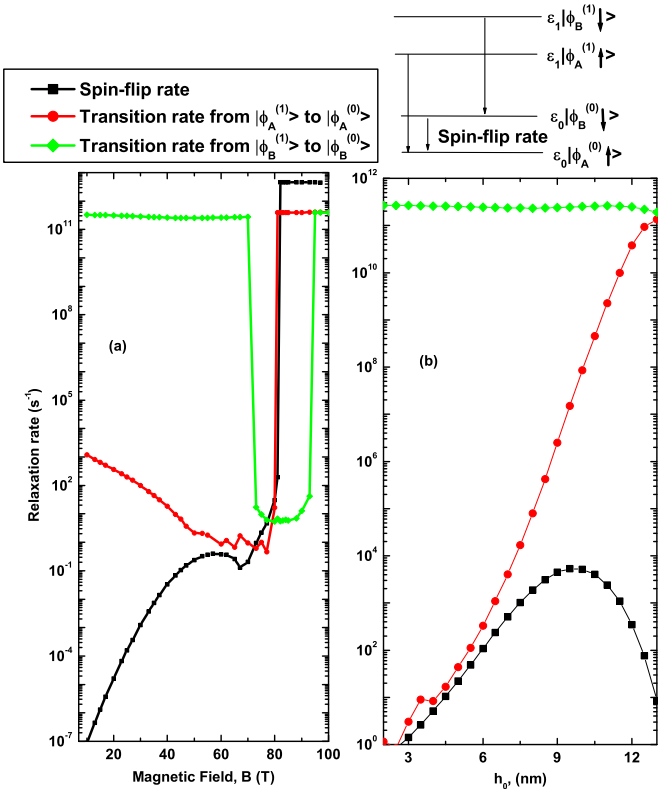

Fig. 6. Spin transition rate vs. magnetic fields (left) and amplitude of out-of-plane ripple waves. Here we chose $h_0 = 1$ nm (left) and $B = 65$ T (right). The parameters are chosen to be the same as Figure 1.

Such spin hot spot possesses very small spin life time and may not be considered as an ideal location for the design of graphene nanoribbon based optoelectronic, spintronic, and straintronic devices for applications such as quantum information processing. Thus one may utilize the external magnetic fields (40 T $\sim$ 60 T is the best operating regime in Fig. 2) smaller than those values of the magnetic fields that induce spin hot spots ($\approx$80 T in Fig. 2) where the strength of pseudomagnetic fields reaches up to $\approx$2000 T (twice as large as those values reported in Ref. [42]). One can reduce the best operating regime of external magnetic fields up to a few tesla by designing strain tensor in GNRs that induces smaller pseudomagnetic fields [27,34]. The level crossing of the triplet orbital states (for energy eigenvalues, see Fig. 2) provides the spin relaxation between singlet ($|\phi_B^{(0)}\downarrow>$) and triplet states ($|\phi_B^{(1)}\uparrow>$ that is shown in Figure 6a (green) between $B = 65$ T and 85 T. In Figure 6b, we have plotted the transition rate between several energy eigenvalues (see the band diagram in Fig. 2) vs. the amplitude of the out-of-plane ripple waves, h_0, where we keep other parameters (such as applied stress, τ_e, magnetic field and in-plane ripple waves) fixed. Here, when we increase the amplitude of out-of-plane ripple waves, h_0, and keep applied stress, τ_e, fixed, we find that the interplay between pseudomagnetic fields due to in-plane and out-of-plane ripple waves and external magnetic fields induces the decreasing values of spin-splitting energy that eventually vanishes at approximately $h_0 = 10$ nm. Thus, due to the principle of conservation of energy, vanishing spin-splitting energy induces negligible photon density of states that provide vanishing spin-flip rates at larger values of the amplitude of the out-of-plane ripple waves.

4 Conclusion

Based on analytical and finite element numerical results, from Figures 1–5, we have analyzed the interplay between the pseudomagnetic fields due to in-plane and out-of-plane ripple waves and externally applied magnetic fields on the band structures of graphene nanoribbons. Here we have shown that the manipulation of spin splitting of graphene electrons (where the level crossing can be observed) is possible by coupling two combined effects: pseudomagnetic fields (originating from ripple waves) and external magnetic fields. In Figure 6, we have shown that the spin relaxation rate is greatly enhanced at the level crossing point (at approximately $B = 65$ T) due to admixture of spin and orbital states. Thus, at the level crossing point, the mixing of spin and orbital states reduces the spin life time. Hence such a point can not be considered an ideal location for the design of graphene nanoribbon based optoelectronic, spintronic, straintronic devices for such applications as quantum information processing. As a result, by understanding the intrinsic features of the ripple waves, one might need to avoid applying the exact magnitude of external magnetic field that mixes the orbital and spin states in graphene nanoribbons for designing straintronic devices. Thus, understanding the influence of ripple waves and magnetic fields on the band structures of graphene might be useful for tuning the bandgaps and level crossing of singlet-triplet states in strained GNRs.

R.M. and S.P. were supported by the Natural Sciences and Engineering Research Council (NSERC) of Canada, the Canada Research Chair (CRC) program. R.M. was supported by the Bizkaia Talent Grant under the Basque Government through the BERC 2014-2017 program, as well as Spanish Ministry of Economy and Competitiveness MINECO: BCAM Severo Ochoa excellence accreditation SEV-2013-0323.

Author contribution statement

Conception of work: S.P., R.M. and L.B. S.P. prepares an initial draft of the work. Data analysis, interpretation, critical revision of the article: S.P., R.M. and L.B.

References

1. S. Das Sarma, S. Adam, E.H. Hwang, E. Rossi, Rev. Mod. Phys. **83**, 407 (2011)
2. A.H. Castro Neto, F. Guinea, N.M.R. Peres, K.S. Novoselov, A.K. Geim, Rev. Mod. Phys. **81**, 109 (2009)
3. K.S. Novoselov, A.K. Geim, S.V. Morozov, D. Jiang, M.I. Katsnelson, I.V. Grigorieva, S.V. Dubonos, A.A. Firsov, Nature **438**, 197 (2005)
4. M. Barbier, P. Vasilopoulos, F.M. Peeters, Phys. Rev. B **81**, 075438 (2010)
5. K.S. Novoselov, D. Jiang, F. Schedin, T.J. Booth, V.V. Khotkevich, S.V. Morozov, A.K. Geim, Proc. Natl. Acad. Soc. **102**, 10451 (2005)
6. K.S. Novoselov, A.K. Geim, S.V. Morozov, D. Jiang, Y. Zhang, S.V. Dubonos, I.V. Grigorieva, A.A. Firsov, Science **306**, 666 (2004)
7. Y. Zhang, Y.-W. Tan, H.L. Stormer, P. Kim, Nature **438**, 7065 (2005)
8. V.B. Shenoy, C.D. Reddy, A. Ramasubramaniam, Y.W. Zhang, Phys. Rev. Lett. **101**, 245501 (2008)
9. S.-M. Choi, S.-H. Jhi, Y.-W. Son, Phys. Rev. B **81**, 081407 (2010)
10. W. Bao, K. Myhro, Z. Zhao, Z. Chen, W. Jang, L. Jing, F. Miao, H. Zhang, C. Dames, C.N. Lau, Nano Lett. **12**, 5470 (2012)
11. E. Cadelano, P.L. Palla, S. Giordano, L. Colombo, Phys. Rev. Lett. **102**, 235502 (2009)
12. W. Bao, F. Miao, Z. Chen, H. Zhang, W. Jang, C. Dames, C.N. Lau, Nat. Nano **4**, 562 (2009)
13. J.C. Meyer, A.K. Geim, M.I. Katsnelson, K.S. Novoselov, T.J. Booth, S. Roth, Nature **446**, 60 (2007)
14. L.L. Bonilla, A. Carpio, Phys. Rev. B **86**, 195402 (2012)
15. F. Guinea, M.I. Katsnelson, A.K. Geim, Nat. Phys. **6**, 30 (2010)
16. M. Gibertini, A. Tomadin, M. Polini, A. Fasolino, M.I. Katsnelson, Phys. Rev. B **81**, 125437 (2010)
17. A.L. Kitt, V.M. Pereira, A.K. Swan, B.B. Goldberg, Phys. Rev. B **85**, 115432 (2012)
18. A. Carpio, L.L. Bonilla, Phys. Rev. B **78**, 085406 (2008)
19. E. Cadelano, L. Colombo, Phys. Rev. B **85**, 245434 (2012)

20. S. Prabhakar, R. Melnik, L.L. Bonilla, S. Badu, Phys. Rev. B **90**, 205418 (2014)
21. L.L. Bonilla, M. Ruiz-Garcia, Phys. Rev. B **93**, 115407 (2016)
22. L.L. Bonilla, A. Carpio, C. Gong, J.H. Warner, Phys. Rev. B **92**, 155417 (2015)
23. E. Cerda, L. Mahadevan, Phys. Rev. Lett. **90**, 074302 (2003)
24. A. Fasolino, J.H. Los, M.I. Katsnelson, Nat. Mater. **6**, 858 (2007)
25. D.V. Tuan, F. Ortmann, D. Soriano, S.O. Valenzuela, S. Roche, Nat. Phys. **10**, 857 (2014)
26. M. Droth, G. Burkard, Phys. Rev. B **84**, 155404 (2011)
27. M. Droth, G. Burkard, Phys. Rev. B **87**, 205432 (2013)
28. L.D. Landau, E.M. Lifshitz, *Theory of Elasticity* (Pergamon Press Ltd., 1970)
29. F. de Juan, J.L. Mañes, M.A.H. Vozmediano, Phys. Rev. B **87**, 165131 (2013)
30. L. Meng, W.-Y. He, H. Zheng, M. Liu, H. Yan, W. Yan, Z.-D. Chu, K. Bai, R.-F. Dou, Y. Zhang, Z. Liu, J.-C. Nie, L. He, Phys. Rev. B **87**, 205405 (2013)
31. F. Guinea, M.I. Katsnelson, M.A.H. Vozmediano, Phys. Rev. B **77**, 075422 (2008)
32. V. Krueckl, K. Richter, Phys. Rev. B **85**, 115433 (2012)
33. S. Prabhakar, R. Melnik, L. Bonilla, Phys. Rev. B **93**, 115417 (2016)
34. N. Levy, S.A. Burke, K.L. Meaker, M. Panlasigui, A. Zettl, F. Guinea, A.H.C. Neto, M.F. Crommie, Science **329**, 544 (2010)
35. F. Guinea, B. Horovitz, P. Le Doussal, Phys. Rev. B **77**, 205421 (2008)
36. L. Brey, H.A. Fertig, Phys. Rev. B **73**, 235411 (2006)
37. J. Klinovaja, D. Loss, Phys. Rev. X **3**, 011008 (2013)
38. A.H. Castro Neto, F. Guinea, N.M.R. Peres, Phys. Rev. B **73**, 205408 (2006)
39. R. Carrillo-Bastos, C. León, D. Faria, A. Latgé, E.Y. Andrei, N. Sandler, Phys. Rev. B **94**, 125422 (2016)
40. D.A. Gradinar, M. Mucha-Kruczyński, H. Schomerus, V.I. Fal'ko, Phys. Rev. Lett. **110**, 266801 (2013)
41. Z. Qi, D.A. Bahamon, V.M. Pereira, H.S. Park, D.K. Campbell, A.H.C. Neto, Nano Lett. **13**, 2692 (2013)
42. W.-Y. He, Y. Su, M. Yang, L. He, Phys. Rev. B **89**, 125418 (2014)
43. D.A. Bahamon, Z. Qi, H.S. Park, V.M. Pereira, D.K. Campbell, Nanoscale **7**, 15300 (2015)
44. E. Merzbacher, *Quantum Mechanics* (John Wiley & Sons, Inc., New York, 2004)